Remote Sensing of Environment 175 (2016) 158–166

Contents lists available at ScienceDirect

Remote Sensing of Environment

journal homepage: www.elsevier.com/locate/rse

Sea–air CO_2 fluxes in the Southern Ocean for the late spring and early summer in 2009

Suqing Xu [a,b,*], Liqi Chen [a], Haiying Chen [c], Jonathan Li [d,e], Wuhui Lin [a,f], Di Qi [a]

[a] Key Laboratory of Global Change and Marine-Atmospheric Chemistry, The Third Institute of Oceanography, State Oceanic Administration, Xiamen 361005, China
[b] State Key Laboratory of Satellite Ocean Environment Dynamics, The Second Institute of Oceanography, State Oceanic Administration, Hangzhou 310012, China
[c] Laboratory of Marine Acoustics and Remote Sensing Technology, The Third Institute of Oceanography, State Oceanic Administration, Xiamen 361005, China
[d] MOE Key Laboratory of Underwater Acoustic Communication and Marine Information Technology, School of Information Science and Engineering, Xiamen University, 422 Siming Road South, Xiamen 361005, China
[e] Department of Geography and Environmental Management, University of Waterloo, 200 University Ave. West, Waterloo, Ontario N2L 3G1, Canada
[f] Department of Engineering Physics, Tsinghua University, Beijing 100084, China

ARTICLE INFO

Article history:
Received 13 March 2015
Received in revised form 27 November 2015
Accepted 31 December 2015
Available online xxxx

Keywords:
Sea-air CO_2 fluxes
Extrapolation method
Remote sensing
The Southern Ocean
CHINARE

ABSTRACT

The Southern Ocean is an important sink of atmospheric carbon dioxide (CO_2). However, the magnitude of the CO_2 sink is uncertain because of the scarcity of in-situ observations due to its remote and rough waters. Empirical relationships were deduced based on the in-situ partial pressure of carbon dioxide (pCO_2) in surface seawater and its main controls including Chlorophyll a (Chl-a) and Sea Surface Temperature (SST) obtained during the 26th CHINARE cruise in late spring (November) and early summer (December) 2009. An extrapolation method based on multiple linear regressions was set up for combining the empirical relationship with satellite data to compute the sea–air carbon fluxes and carbon uptake in the Southern Ocean (south of 50°S). The empirical relationships are validated with independent measurements from SOCATv2 database. The mean standard deviation differences (Std) between extrapolated and measured pCO_2 from SOCATv2 database (13.8 to 18.1 μatm) are consistent with the precision of our regressions (13.6 to 21.3 μatm). Including the effects of sea ice, we estimate a Southern Ocean CO_2 source to the atmosphere in November 2009 about 1.65 Tg C with an uncertainty of ±0.73 Tg C by uncertainty propagation formula. While in December 2009, we estimated a CO_2 sink of −2.34 Tg C with an uncertainty of ±1.03 Tg C. The carbon source and sink of the South Atlantic Ocean, the South Indian Ocean and the South Pacific Ocean were estimated. For the austral summer, the South Atlantic Ocean and the South Pacific Ocean are still strong carbon sink. When compared to the climatological monthly results of Takahashi et al. (2012), our results showed a similar distribution of sea–air carbon flux.

1. Introduction

The Southern Ocean, defined here as the oceanic region south of 50°S, is a major region for the formation of deep-water masses that fill the ocean basins. It is a key region in the global uptake of anthropogenic carbon dioxide (CO_2) (Sabine et al., 2004). The Southern Ocean is regarded as a small sink on an annual average despite the fact that the source-sink conditions vary over a wide range through the seasons (Takahashi et al., 2012). Estimates based on models are subject to considerable biases due to sparse in-situ collection and the complexity of processes controlling surface water CO_2 levels, including physical mixing, sea ice conditions, wind regimes and biological interactions. The carbon uptake capacity varied sharply from 0.05 to 0.7 $PtCyr^{-1}$ between models and observations in the Southern Ocean (Tans, Fung, & Takahashi, 1990; Winguth et al., 1994; Takahashi et al., 1997; Louanchi et al., 1999; Louanchi & Hoppema, 2000; Takahashi et al., 2002; Sabine et al., 2004; Bender et al., 2005; McNeil, Metzl, Key, Matear, & Corbiere, 2007; Quay et al., 2007; Takahashi et al., 2009; Gruber et al., 2009; Le Quéré, Takahashi, Buitenhuis, Rödenbeck, & Sutherland, 2010; Lenton et al., 2013).

In an austral summer, with increasing heating due to solar radiation, sea surface temperature (SST) rises, sea ice melts, biological productivity increases and, with enhanced open water, the Southern Ocean turns to be the strongest sink of the year in the Polar Frontal Zone (PFZ) and Antarctic Zone (AZ) (Lenton et al., 2013; Metzl, Tilbrook, & Poisson, 1999; Takahashi et al., 2009, 2012). Despite its importance, the Southern Ocean remains one of the poorly sampled ocean regions with respect to CO_2. It is difficult to accurately determine the carbon absorption in warmer seasons.

The objective of our study was to determine the spatiotemporal distribution of the sea–air CO_2 flux and carbon uptake in late spring (November) and early summer (December) in the Southern Ocean. This study focuses on the area south of 50°S to the ice edge during the

* Corresponding author at: No.178 Daxue Road, Xiamen, Fujian, 361005, PR China.

http://dx.doi.org/10.1016/j.rse.2015.12.049
0034-4257/

26th CHINARE (Chinese National Antarctic Research Expedition) campaign. The R/V Xuelong sailed along the marginal ice zone (moving clockwise from 180°W to 90°W) and arrived at Changcheng Station in late spring 2009. After a few days break, the R/V Xuelong sailed toward the Zhongshan Station (moving clockwise from 0°E to 90°E) in early summer 2009 (see Fig. 1).

Our methodology to estimate the sea–air CO_2 flux consists of the following steps:

(1) To create the empirical relationships for the partial pressure of carbon dioxide (pCO_2) and Chl-a and SST by multiple linear regression (MLR) from the in-situ underway measurements collected during the 26th CHINARE campaign in the Southern Ocean,
(2) To produce pCO_2 in surface seawater (pCO_2^{sw}) by the empirical relationships via remotely sensed Chl-a and SST data and to conduct a validation by independent data from the SOCATv2 database,
(3) To estimate sea–air CO_2 flux by combining the difference of pCO_2, and the gas exchange velocities on each pixel including the effect of sea ice,
(4) To compare the carbon capacity in the South Atlantic Ocean, the South Indian Ocean and the South Pacific Ocean and to other estimate, and
(5) To analyze uncertainty and related errors in the MLR extrapolation method of sea–air CO_2 flux.

2. Data

2.1. In situ data

pCO_2^{sw} data was obtained along the cruise by an automated underway pCO_2 observation system (GO Flowing pCO_2 system, General Oceanics Inc., Miami FL, USA) which was installed onboard the R/V Xuelong icebreaker (see Fig. 2). Seawater was pumped continuously from a side intake 4 m below sea surface to the laboratory and then sprayed through a showerhead into a gas-water equilibration chamber. At a rate of approximately 1 L min^{-1} the seawater was pumped in to the cooler extractor and then into the infrared analyzer (LICOR, USA, Model 7000). The analyzer was calibrated every 2.5–3 h using four CO_2 standard gases at pressures of 244.25 ppm, 546.98 ppm, 420.56 ppm, and 366.86 ppm supplied by NOAA's Global Monitoring Division. The accuracy of the reported pCO_2^{sw} is within 2 μatm (Pierrot et al., 2009). Marine air was pumped from the crow's nest into the ship laboratory through plastic tubing, which was flushed continuously until a subsample was taken. After that it was pumped into the cooler extractor and then into the infrared analyzer (LICOR, USA, Model 840). The underway atmospheric pCO_2 (pCO_2^{air}) have been filtered and compared with the measurements from the monitoring stations from WDCGG located around the Antarctica continent as shown in Fig. 2. The distribution of pCO_2 in both sea water and atmosphere was shown in Fig. 3-a.

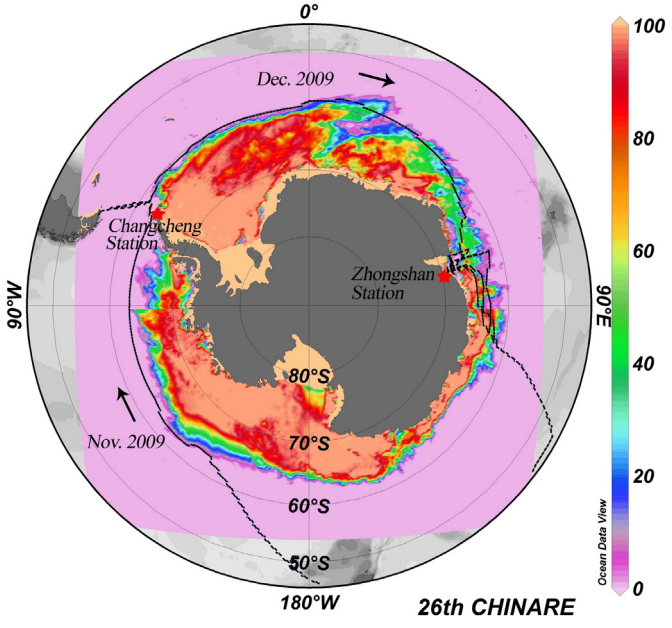

Fig. 1. Distribution of sea ice coverage (%) from NSIDC during the 26th CHINARE campaign. The black lines represent the cruise of R/V Xuelong and the black arrows show the directions.
Schlitzer, ODV3.4.3 (2009).

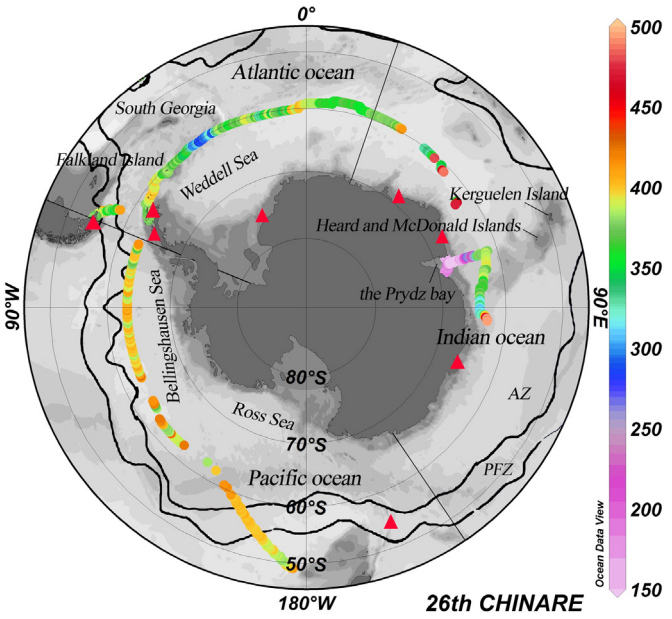

Fig. 2. The underway measurements of pCO_2^{sw} (μatm) along the cruise (data eastward of 90°E was not shown since it was collected in January 2010); red triangles present the distribution of the atmospheric CO_2 sites around the Antarctica from WDCGG. Overlain on these figures, from north to south are the mean positions of the major zones: the Polar Front Zone (PFZ) and the Antarctica Zone (AZ) following Orsi, Whitworth, and Nowlin (1995).
Schlitzer, ODV3.4.3 (2009).

Water Chl-a samples were taken four times a day from the sea surface during the course of the experiment using plastic cask water samplers. Surface sea water sample (500 ml) was filtered through a GF/F filter. After then, the filters were extracted with 90% acetone in darkness at −20 °C for 24 h. The Chl-a concentrations were determined using a Turner Designs fluorometer (Model II) with a precision of ±10%. Sea surface temperature was measured using a SeaBird conductivity, temperautre and depth (CTD) profiler SBE 45 and the precision was ±0.01 °C. The distributions of in-situ SST and Chla along the cruise track were shown in Fig.3-b.

2.2. Satellite data

Remotely sensed Chl-a and SST data were downloaded from the Aqua MODIS instrument (http://oceancolor.gsfc.nasa.gov) with a spatial resolution of 4 km (see Figs. 4 and 5). Monthly Chl-a and SST fields were interpolated to be 1°long by 0.25°lat grid resolution to extrapolate pCO_2^{sw}. In order to test the accuracy of remotely sensed Chl-a and SST, we downloaded daily data from Aqua MODIS. Due to cloud cover and orbit gap, we selected the remotely sensed data close to the in-situ data at 4 km limit. The correlation of remotely sensed and the in-situ Chl-a was 65% and correlation of SST was 12%. Remotely sensed wind speed from NASA ASCAT L2 product with a spatial resolution of

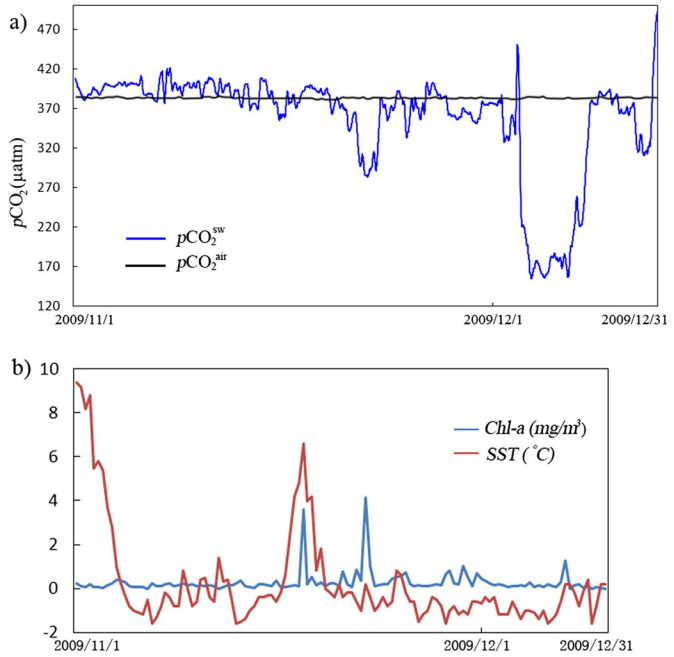

Fig. 3. a) Distributions of underway pCO_2 (μatm) in sea water and atmosphere along the cruise track in November and December 2009; b) Distributions of in-situ SST (°C) and Chl-a (mg/m^3) along the longitudinal shift. In-situ SST data were interpolated to match the sampling frequencies of Chl-a.

12.5 km (see Fig. 6) was downloaded to derive the sea–air gas exchange coefficient to estimate the sea–air CO_2 flux. The accuracy of the wind speed of ASCAT product is high when it is away from coast and beyond 3 m s^{-1} and the overall correlation is 94% between buoy data and ASCAT product (Xie, Wei, & Huang, 2014). To incorporate the effect of sea ice, the CO_2 flux was assumed proportional to the percent ice-free area (Worby et al., 2008). Sea ice concentrations (see Fig. 1) were downloaded from AMSR-E with a spatial resolution of 12.5 km.

3. Methodology

3.1. Empirical relationship of pCO_2 with Chl-a and SST

In the Southern Ocean, it has been reported that Chl-a and SST are the major factors influencing the spatiotemporal variation of sea surface pCO_2 (Bates, Hansell, Carlson, & Gordon, 1998a; Bates, Takahashi, Chipman, & Knap, 1998b; Metzl et al., 1999; Sweeney, 2002; Barbini et al., 2003; Hales & Takahashi, 2004; Rangama et al., 2005; Chen et al., 2011).

In our previous work from the underway measurements conducted in the 16th and the 21st CHINARE, we found that marine pCO_2 correlated negatively with Chl-a in the South Atlantic Ocean and the South Indian Ocean, and showed negative correlation with respect to SST in upwelling zones (Chen et al., 2011). The pCO_2–Chl-a relationships were used to take into account of the biological effects while the use of SST considered the mixing, upwelling and the thermodynamic effects to be taken into account.

Biological contribution may be more evident in a SST dominating region since the biological activity tends to be higher in warm water while a physical contribution may be included in a chlorophyll dominating region as well since mixing affects biology (Rangama et al., 2005). In this study, to account for different sampling frequencies, the underway pCO_2^{sw} and SST data were selected to match the Chl-a data to an optimal interval. When all underway measurements obtained in the 26th CHINARE were analyzed, we tested linear fits between pCO_2 and SST and between pCO_2 and Chl-a (see Fig. 7). We found that pCO_2^{sw} showed a different relationship with Chl-a and SST depending on regional Chl-a value (see Table 1). We empirically derived a Chl-a threshold of 0.5 mg m^{-3}. pCO_2^{sw} correlated negatively with Chl-a in the region where Chl-a value was greater than 0.5 mg m^{-3} during the study period. When Chl-a values were smaller than 0.5 mg m^{-3}, pCO_2, Chl-a and SST are analyzed by Sigmaplot (a statistical software package) using the MLR algorithm. We found that pCO_2 is related to Chl-a and SST, with R^2 of 0.6321 and 0.7649 for November and December 2009, respectively. Deduced empirical relationships of pCO_2 with Chl-a and SST are listed in Table 2.

3.2. Sea–air CO_2 flux calculation and carbon uptake estimation

The difference between pCO_2 ($\Delta pCO_2 = [(pCO_2)^{sw} - (pCO_2)^{air}]$), determines the direction of CO_2 transfer across the sea surface. The sea–air CO_2 flux is classically estimated from sea–air gas transfer velocity (K) and ΔpCO_2 according to Wanninkhof (1992):

$$\text{Flux} = K \times L \times (\Delta pCO_2) \quad (1)$$

where K is the gas transfer velocity (in cm h^{-1}), a quadratic relationship of wind speed (U_{10} in unit of m s^{-1}) and the Schmidt number expressed as $(Sc/660)^{-0.5}$. L is the solubility of CO_2 in seawater (in mol liter^{-1} atm^{-1}) (Weiss, 1974). For a monthly estimation and wind speed range of 3–15 ms^{-1} or higher the scaling factor for the gas transfer

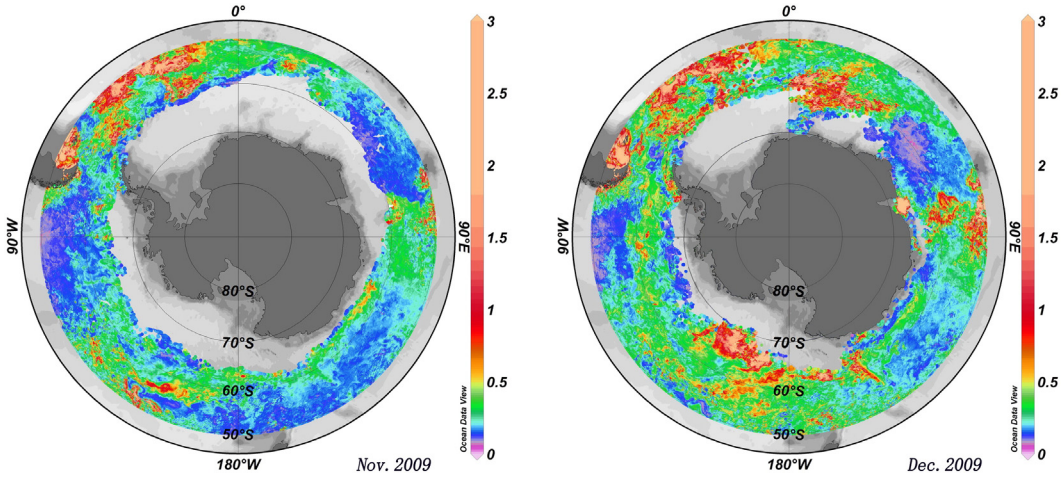

Fig. 4. Aqua-Modis chlorophyll-a (mg/m^3) images for November and December 2009. Schlitzer, ODV3.4.3 (2009).

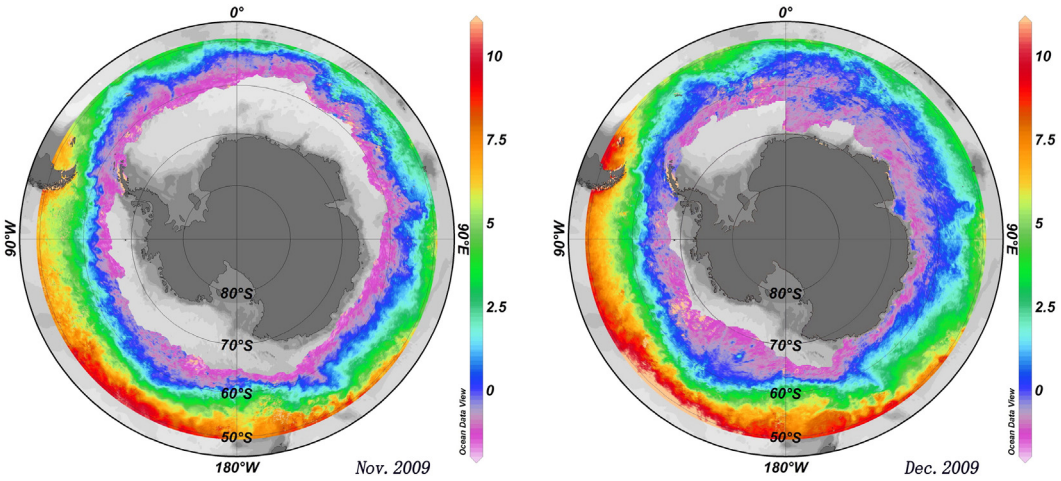

Fig. 5. Aqua-Modis sea surface temperature (°C) images for November and December 2009. Schlitzer, ODV3.4.3 (2009).

rate is 0.251, which has a 20% uncertainty (Wanninkhof, 2014; Wanninkhof, Asher, Ho, Sweeney, & McGillis, 2009). Taking into account the unit conversion factor (Takahashi et al., 2009) Eq. (1) can be simplified as:

$$\mathrm{Flux}_{\mathrm{sea-air}}\left(\mathrm{g\ Cm^{-2}\ month^{-1}}\right) = 7.7 \times 10^{-4} \times U^2 \times (\Delta p\mathrm{CO_2}). \qquad (2)$$

Monthly sea–air CO_2 flux in the Southern Ocean can be estimated by Eq. (2) proportional to the percent ice-free area within each grid box (Takahashi et al., 2012). Remote sensing data of wind speed and ice concentration were interpolated to be 1°long by 0.25°lat grid resolution. pCO_2^{air} data of the same grid resolution was produced by linearly regressing the underway pCO_2 in atmosphere along the cruise track. The total carbon uptake was then obtained by summing up the fluxes of each grid by each area according to Jiang, Cai, Wanninkhof, Wang, and Lüger (2008).

4. Results and discussion

4.1. Quality and maps of extrapolation of pCO_2^{sw}

The weakness of the extrapolation method is that it is based on limited cruises of underway measurements and extrapolation to areas without any actual measurements or undersampling. In order to validate the accuracy of extrapolated pCO_2^{sw}, we search independent measurements from the to-date largest sea surface pCO_2 observation database (Surface Ocean CO_2 Atlas version 2, http://www.socat.info/) (Bakker et al., 2014). Data from the SOCATv2 database was scarce during our study period (see Fig. 8). Data from the south of Argentina (around 50°S) to the Antarctic Peninsula (around 67°S) were partly overlain with our cruise tracks. We applied the pCO_2 empirical relationships using SST downloaded together from the SOCATv2 database and weekly chlorophyll-a data from Aqua MODIS at 4 km resolution to compute extrapolated pCO_2^{sw}. Data of fugacity of CO_2 from SOCATv2 database were calculated to be pCO_2 according the fugacity correction (Pierrot et al., 2009). Extrapolated and measured pCO_2 from SOCATv2 database were plotted against each other (see Fig. 9a, b) and the overall standard deviation was 13.8 and 18.1 μatm for November and December 2009, which were consistent with the precision of our regressions (13.6 to 21.3 μatm). In the South Indian Ocean in November 2009 and in the South Pacific Ocean in December 2009 where there were no actual samples, validation between extrapolated pCO_2^{sw} and measured pCO_2 from SOCATv2 (see Fig. 9-c, d) resulted in the standard deviation of 14.5 and 16.5 μatm respectively. These gave credibility to our MLR extrapolation method. This result is encouraging especially in the Southern Ocean where scarce in-situ measurements were obtained.

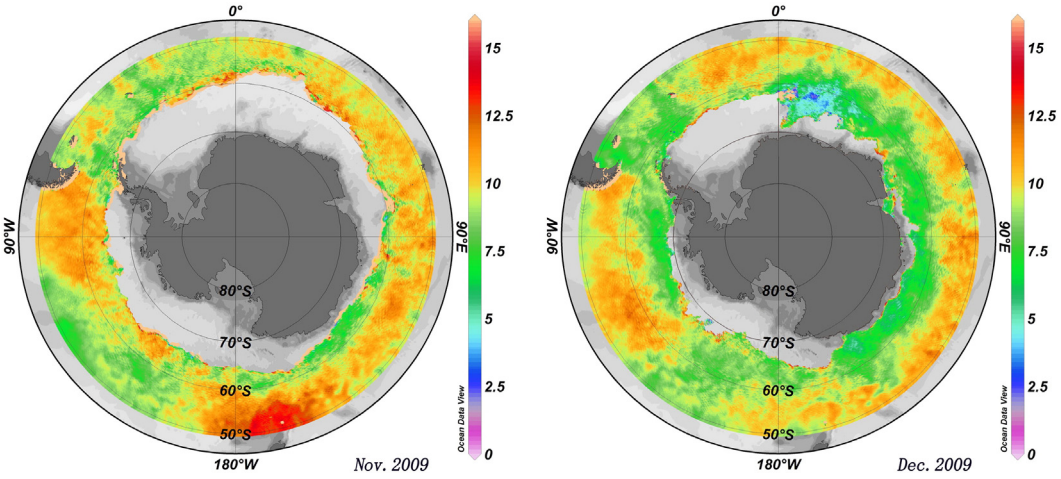

Fig. 6. ASCAT mean wind speed (m/s) at 10 m above the sea surface water images for November and December 2009. Schlitzer, ODV3.4.3 (2009).

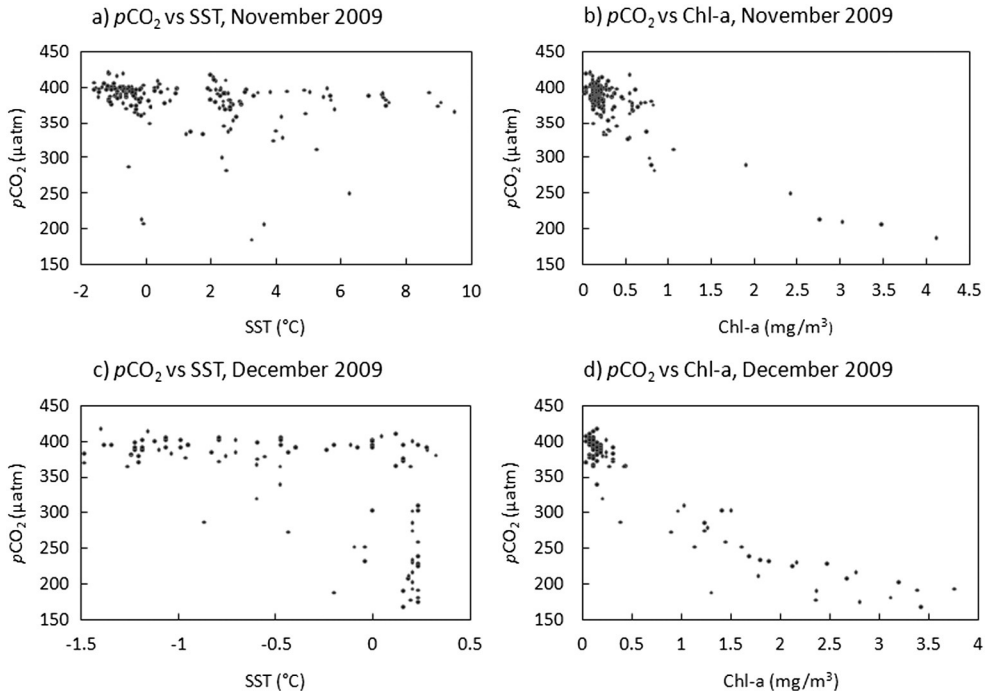

Fig. 7. Relationships between pCO_2 and SST for November 2009 (a) and for December 2009 (c); relationships between pCO_2 and Chl-a for November 2009 (b) and for December 2009 (d).

Our results show strong regional variation of pCO_2^{sw} in both temporal and spatial structure. Monthly 1°long × 0.25°lat extrapolated pCO_2^{sw} maps for November and December 2009 are shown in Fig. 10. In November 2009, that was late spring of the year in the Southern Ocean, when sea ice began to melt, SST in the Southern Ocean showed a strong north–south gradient (see Fig. 5). Aqua-Modis Chl-a images (see Fig. 4) showed that biological productivity was low with an average remotely sensed Chl-a of 0.22 mg m^{-3} in the Indian Ocean sector and the Pacific Ocean sector except in the Atlantic Ocean sector Chl-a values beyond 1 mg m^{-3} were found. pCO_2^{sw} was high in the chlorophyll-poor areas and low in the chlorophyll-rich areas. In most part of the area in the Indian Ocean sector and the Pacific Ocean sector, pCO_2^{sw} exceeded the mean atmospheric pCO_2 of 385.25 µatm. While in the Atlantic Ocean sector, pCO_2^{sw} below 300 µatm was founded in the area from 14°W to 46°W, 55°S to 60°S.

In December 2009, the austral summer was initiated based on climatologic statistics in the Southern Ocean. With the increasing sunlight, sea ice decreased around the Antarctic continent. SST increased by an average of 0.67 °C compared to November 2009. Stable mixed layers and sea-ice dynamics promote considerable biological production in the AZ. The productivity in the region increased considerably compared to November 2009, and pCO_2^{sw} correspondingly decreased especially along the sea ice retreat trend. The average Chl-a value from remotely sensed data was 0.46 mg m^{-3}, in most parts of the Atlantic Ocean, the Chl-a value exceeded 1 mg m^{-3}. In the chlorophyll-poor areas in the Pacific Ocean sector pCO_2^{sw} exceeded 400 µatm. In the majority part of the Indian Ocean sector, pCO_2^{sw} was close to or beyond atmospheric pCO_2.

4.2. Spatiotemporal distribution of sea–air CO_2 flux

Fig. 11 shows the monthly 1°long × 0.25°lat sea–air CO_2 fluxes in November and December 2009 from the product of monthly wind speed and monthly ΔpCO_2 grids at the same resolution. In November 2009, the area south of 50°S is mainly a carbon source with an average carbon flux of 1.07 gC m^{-2} $month^{-1}$. In the South Pacific Ocean, high wind speed values around 15 m/s occurred from 160°E to 175°E, 50°S to 55°S (see Fig. 6). High speed winds strengthened the carbon source and the South Pacific Ocean sector is the strongest source with an average flux of 1.8 gC m^{-2} $month^{-1}$ and the total carbon release is 1.06 Tg C (1 T = 10^{12} g). In the South Indian Ocean, except the areas around the Kerguelen Island and the Heard and McDonald Islands came into being a weak carbon sink due to phytoplankton bloom in late spring (Blain et al., 2007), the South Indian Ocean sector is the second carbon

Table 1
Linear regression of pCO_2 (µatm) with Chl-a (mg m^{-3}) and SST (°C).

			Nov. 2009	Dec. 2009
Chl-a ≥ 0.5 mg m^{-3}	Chl-a	r	−0.89	−0.86
		α	0.001	0.001
	SST	r	−0.48	−0.43
		α	0.01	0.01
Chl-a < 0.5 mg m^{-3}	Chl-a	r	−0.53	−0.57
		α	0.001	0.001
	SST	r	−0.24	−0.30
		α	0.01	0.01

Here, r is the related coefficient, α is the significance level.

Table 2
Empirical relationship of pCO_2 (µatm) with Chl-a (mg m^{-3}) and SST (°C).

Date	Empirical relationship	Data no.	Std (µatm)
Nov. 2009	$pCO_2\_sw = -57.40 \times$ Chl-a + 394.97 (Chl-a ≥ 0.5)	26	13.6
	$pCO_2\_sw = -74.24 \times$ Chl-a-2.96 × SST + 406.51 (0 < Chl-a < 0.5)	102	21.3
Dec. 2009	$pCO_2\_sw = -44.15 \times$ Chl-a + 328.27 (Chl-a ≥ 0.5)	28	18.2
	$pCO_2\_sw = -134.95 \times$ Chl-a + 0.83 × SST + 408.22 (0 < Chl-a < 0.5)	65	19.6

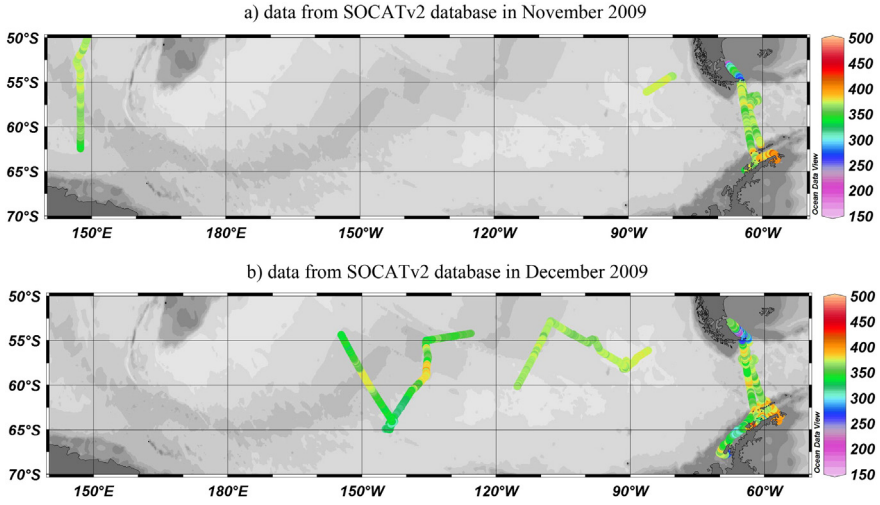

Fig. 8. The distribution of fCO_2 (μatm) from the SOCATv2 database in November and December 2009 for validation of the extrapolation method. (Schlitzer, ODV3.4.3, 2009).

source with an average flux of 0.87 gC m^{-2} $month^{-1}$ and the total carbon release of 0.80 Tg C. While in the Atlantic Ocean sector a carbon sink was found from 50°W to 10°W and the area around southern part of Argentina with a maximum flux of −12.24 gC m^{-2} $month^{-1}$. The total uptake in the South Atlantic Ocean is −0.21 Tg C with an average flux of −0.27 gC m^{-2} $month^{-1}$ (see Table 3). From our calculation, the region south of 50°S was a carbon source and released 1.65 Tg C in November 2009.

In December 2009, when sea surface temperature increased, continental runoff of nutrients from islands and blooms of ice algae in the sea ice margins, made the region a relatively strong carbon sink in the area around islands and where sea ice declined (Arrigo, Worthern, Schnell, & Lizotte, 1998; Atkinson et al., 2001). The strongest sink area existed from 10°W to 40°W, 50°S to 56°S in the South Atlantic Ocean sector with the sea–air flux reaching −21.73 gC m^{-2} $month^{-1}$ where existed a high wind speed of 15.41 m s^{-1} and a high Chl-a value of 1.6 mg m^{-3}. In the South Indian Ocean, area from 80°E to 92°E, 50°S to 55.5°S became a strong sink of CO_2 with a maximum flux of −15.39 gC m^{-2} $month^{-1}$ where existed a wind speed of 10.91 m s^{-1} and a Chl-a value of 2.68 mg m^{-3}. It was also related to iron fertilized Kerguelen bloom during austral summer (Jouandet et al., 2008). The interior part of Prydz Bay region in Antarctica was a strong CO_2 sink with a maximum flux of −24.92 gC m^{-2} $month^{-1}$ due to the highest productivity as shown in Fig.4 the averaged Chl-a value exceeded 3 mg m^{-3}. Most of the areas with strong CO_2 sink were linked with chlorophyll-rich areas.

In the Pacific Ocean sector, from143°W to 169°W, 65°S to 70°S, strong sea–air carbon flux occurred with a maximum flux of −15.39 gC m^{-2} $month^{-1}$ where high Chl-a value beyond 3 mg m^{-3} was found from the satellite image (Fig.4). However in the South Indian sector, from 47°E to 80°E and 110°E to 146°E and in the Pacific Ocean sector, from 80°W to 100°W, there existed a weak source. These areas were associated with chlorophyll-poor regions. The South Atlantic Ocean was the strongest carbon sink with a carbon uptake of −1.61 Tg C despite having the smallest area. The second is the South Pacific Ocean with a carbon uptake of −0.64 Tg C, and then the South

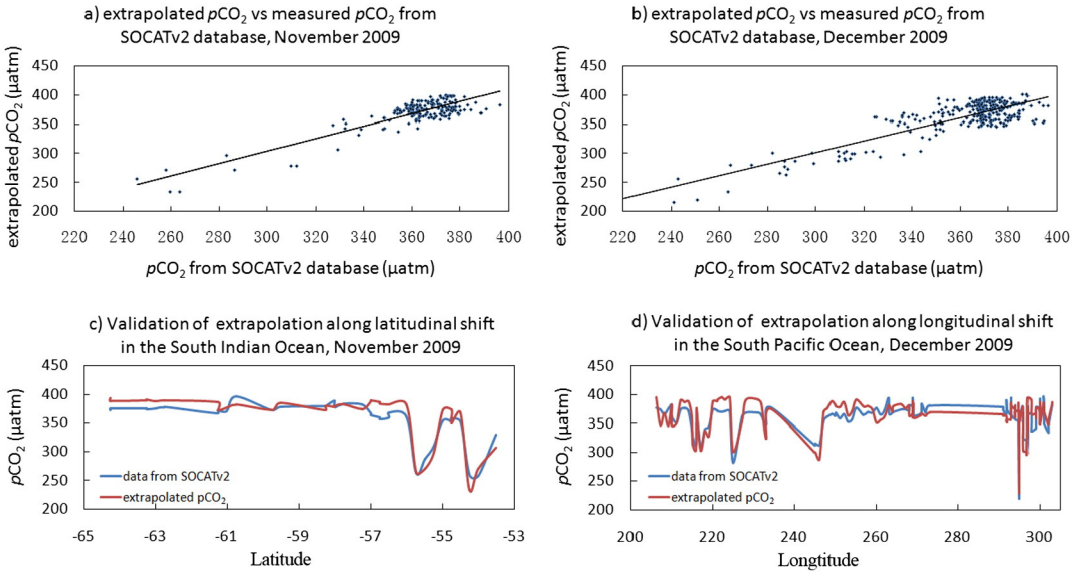

Fig. 9. Validations of the extrapolated pCO_2 vs measured pCO_2 from SOCATv2 database for November 2009 (a) and for December 2009 (b); Validation of extrapolation along latitudinal shift in the South Indian Ocean for November 2009 (c) and along longitudinal shift in the South Pacific Ocean for December 2009 (d).

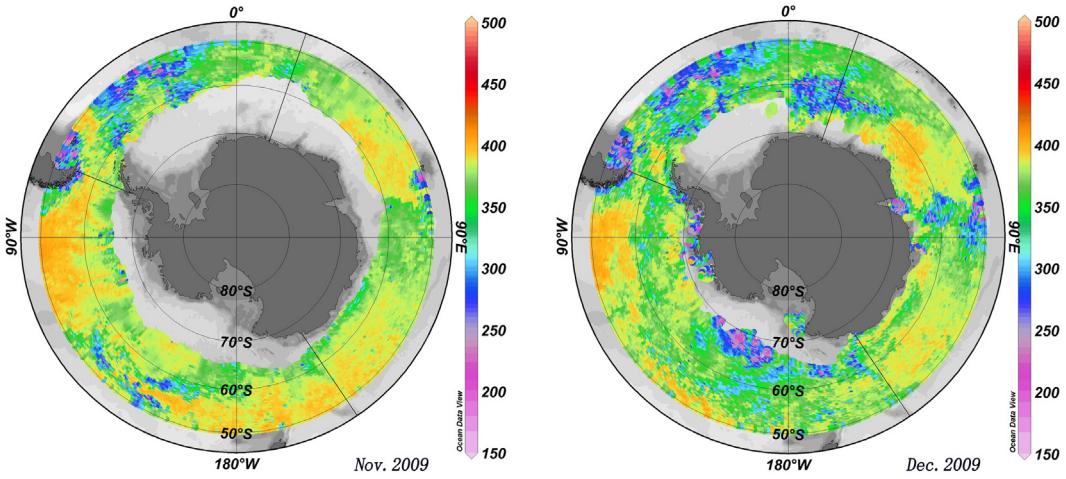

Fig. 10. Extrapolated pCO_2^{sw} (μatm) maps in November and December 2009. Schlitzer, ODV3.4.3 (2009).

Indian Ocean of −0.09 Tg C. In December 2009, carbon absorption was −2.34 Tg C in the Southern Ocean.

4.3. Comparison with climatological estimate

As summarized in Lenton et al. (2013), observations, models and inversions show that the median annual sea–air CO_2 fluxes vary from −0.27 to −0.43 Gt C per year for the entire region from 44°S to 75°S. There are great differences in the studies on carbon flux in the Southern Ocean south of 50°S. Based on about 1.1 million measurements of surface water pCO_2 database in the Southern Ocean (Takahashi et al., 2009; Takahashi et al., 2012), the climatological monthly distributions for sea–air pCO_2 difference at a 4°lat × 5°long resolution warrant a comparison to our empirically derived estimates. Compared to the same months in the reference year 2000 (see Fig. 12), despite different sea ice edge of different year, our results showed a similar distribution of the difference of sea–air pCO_2. In November, the majority of the South Atlantic Ocean was a carbon sink while the South Pacific Ocean and South Indian Ocean were mainly a carbon source. In December, the early summer, the Ross and Weddell Seas and the coastal waters around the Kerguelen and the Heard and McDonald Islands were strong CO_2 sinks. In the Southern Ocean, when winter sea ice starts to melt in the spring, phytoplankton blooms, fueled by high nutrient concentrations, pCO_2 in sea water was rapidly reduced (Bakker, Hoppema, Schröder, Geibert, & de Baar, 2008). The comparison indicates that the spatiotemporal distribution of sea–air carbon flux can be made by empirically derived extrapolation method in the Southern Ocean in warm season.

4.4. Uncertainties of the sea–air CO_2 flux estimation

There are three issues that could lead to systematic error in our sea–air flux estimation. First, the extrapolation method of pCO_2 and Chl-a and SST. Empirical relationships were deduced from underway pCO_2^{sw} and Chl-a, SST. While the use of basin-scale monthly gridded satellite Chl-a and SST images appears to smooth out some of the small-scale spatial variability. Over the Southern Ocean, the mean Std in regressing pCO_2^{sw} were 17.45 and 18.9 μatm, respectively for November and December 2009. Secondly, the use of the chosen gas transfer coefficient could also contribute to systematic biases and accounts for 20% uncertainty (Wanninkhof, 2014). Finally, when the sea–air flux computation expression was simplified, a 1.39% uncertainty occurs.

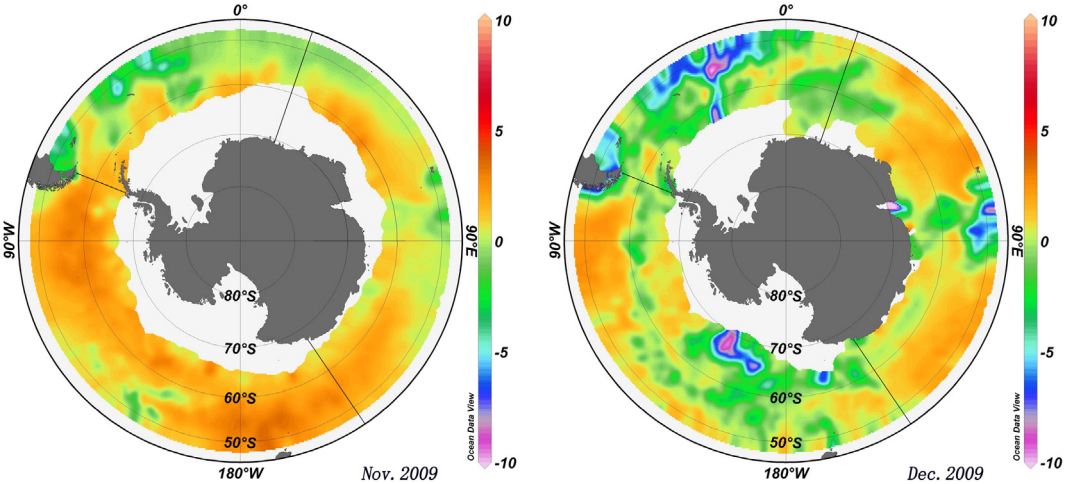

Fig. 11. Spatial and temporal distribution of sea–air carbon flux (negative into the ocean) (gC m^{-2} $month^{-1}$) in the Southern Ocean in November and December 2009. Schlitzer, ODV3.4.3 (2009).

Table 3
Sea–air carbon fluxes (negative into the ocean) in the Atlantic, Indian and Pacific sectors of the Southern Ocean (from 50°S to sea ice edge) in November and December 2009.

	South Atlantic Ocean 67°W–20°E (11.6×10^6 km^2)		South Indian Ocean 20°E–146°E (13.9×10^6 km^2)		South Pacific Ocean 146°E–67°W (18.5×10^6 km^2)	
	Average flux (gC/m^2*mon)	Total uptake Tg	Average flux (gC/m^2*mon)	Total uptake Tg	Average flux (gC/m^2*mon)	Total uptake Tg
2009.11	−0.27	−0.21	0.87	0.80	1.80	1.06
2009.12	−1.79	−1.61	0.36	−0.09	−0.41	−0.64

Uncertainties of the sea–air CO_2 fluxes also arise from the error or bias in the satellite data. The satellite data is useful for identifying oceanic characteristics over the whole area. Errors or biases in the extrapolated pCO_2^{sw} values are introduced because of differences between the satellite-derived data and the in-situ measurements. The precisions of the satellite data including Chl-a, SST, and wind speed show uncertainties of 35%, 12% and 6%, respectively. Apparently the precision of remotely sensed Chl-a is the key factor to determine the precision of extrapolated pCO_2^{sw} and sea–air carbon flux. Uncertainty from the interpolation of the underway atmospheric pCO_2 is regular and small and less than 1% and should not introduce significant systematic error.

According to Eq. (2), the uncertainty of CO_2 flux (F_{error}) can be calculated by Taylor (1997)

$$\frac{F_{error}}{F} = \sqrt{0.2^2 + 4 \times 0.06^2 + 0.0139^2 + \left(\frac{\partial \Delta pCO_2}{pCO_2^{sw} - pCO_2^{air}}\right)^2} \quad (3)$$

where F is the sea–air CO_2 flux; $\frac{\partial \Delta pCO_2}{pCO_2^{sw} - pCO_2^{air}}$ means relative uncertainty from sea–air pCO_2 gradient which was contributed by the uncertainties of remote sensing Chl-a and SST data and the precision of the empirical relationships. The final sea–air CO_2 flux was estimated at an uncertainty of 44%. The final integrated uncertainty estimate is ±0.73 Tg C/month for November 2009 and ±1.03 Tg C/month for December 2009.

5. Conclusion

Up to date, there is scarce sampling on carbon cycle in the Southern Ocean because of its remoteness and atrocious weather. By using satellite-based data, the low-spatial resolution underway pCO_2 data of limited cruises in surface sea water may be extrapolated in space and time to yield pCO_2^{sw} distribution maps with greater resolutions though potential biases would be invoked. In this study we have applied a MLR extrapolation method to estimate the spatiotemporal distribution

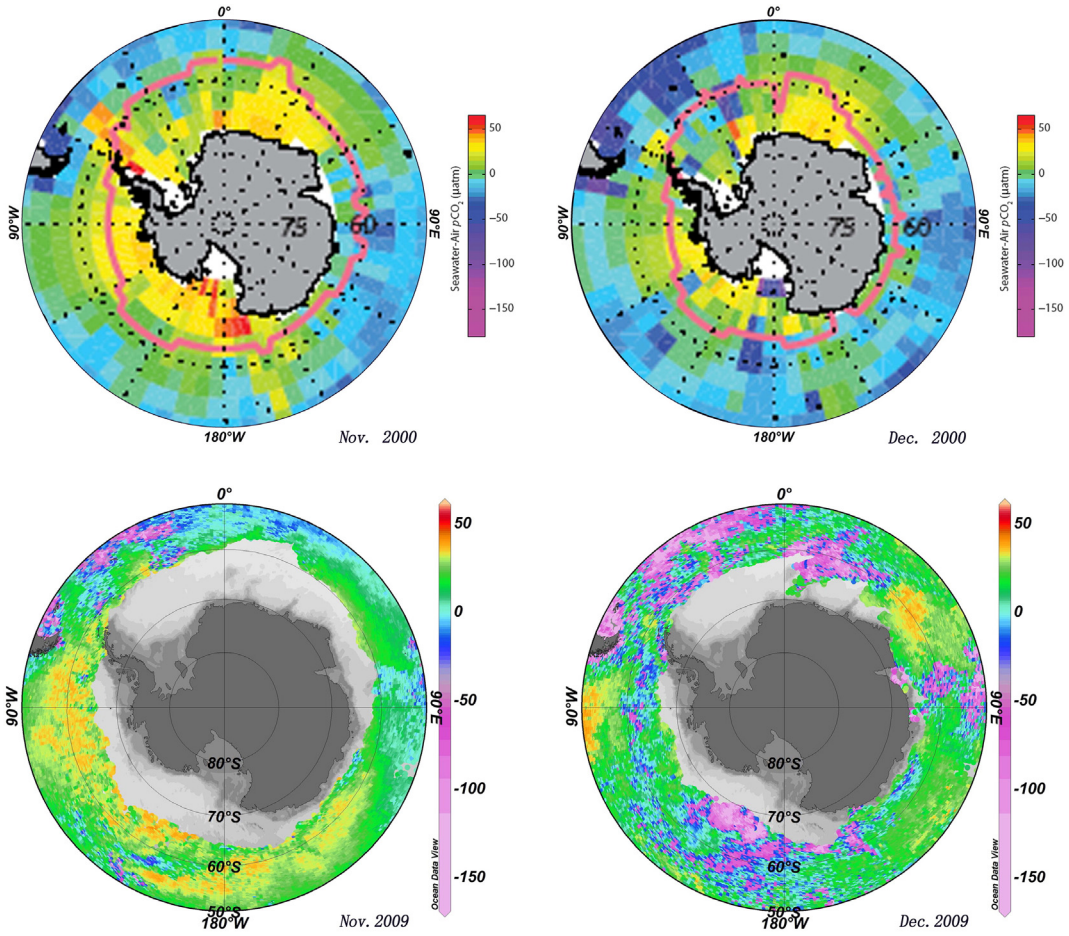

Fig. 12. The comparison of the difference of sea–air pCO_2 between climatological results of Takahashi et al. (2012) (top) and this study (bottom) for the same months. Schlitzer, ODV3.4.3 (2009).

of sea–air carbon flux and the total carbon uptake in the Southern Ocean during the 26th CHINARE campaign in 2009. According to propagation of uncertainty, the uncertainty of our approach was discussed and analyzed. In November 2009 (late spring), the Southern Ocean was a carbon source of 1.65 ± 0.73 Tg C while in December 2009 (early summer), it turned to be a carbon sink of −2.34 ± 1.03 Tg C. From the distribution of extrapolated pCO_2^{sw} and sea–air carbon flux, we found that biological activities were the dominant controlling factor when Chl-a value is above a given threshold in the marine ice zone in the Southern Ocean in warm season. Additionally, the precision of remotely sensed Chl-a is the key factor to determine the precision of extrapolated pCO_2^{sw} and final carbon flux. Comparison among three ocean sectors showed that the South Atlantic Ocean and the South Pacific Ocean turned to be a strong sink in early summer. When compared to the climatological monthly results of Takahashi et al. (2012), our results showed a similar distribution of sea–air carbon flux.

Acknowledgments

This work was partially supported by the National Natural Science Foundation of China under grants 41230529, 41476172 and 41506209, the Open Fund of the State Key Laboratory of Satellite Ocean Environment Dynamics under contract SOED1506, the Chinese Projects for Investigations and Assessments of the Arctic and Antarctic under grants CHINARE2012-15 for 01-04-02, 02-01, and 03-04-02, and the Chinese International Cooperation Projects under grants 2015DFG22010, ISOCORE2011-2015, IC201201, IC201308, and IC201513. We would like to thank the Institute of Oceanology, Chinese Academy of Sciences for providing the Chl-a data. We also thank Rik Wanninkhof of the NOAA/AOML, Miami, USA for his suggestions and comments.

References

Arrigo, K. R., Worthern, D., Schnell, A., & Lizotte, M. P. (1998). Primary production in Southern Ocean waters. *Journal of Geophysical Research*, *103*, 15,587–15,600.

Atkinson, A., Whitehouse, M. J., Priddle, J., Cripps, G. C., Ward, P., & Brandon, M. A. (2001). South Georgia, Antarctica: a productive, cold water, pelagic ecosystem. *Marine Ecology Progress Series*, *216*, 279–308.

Bakker, D. C. E., Hoppema, M., Schröder, M., Geibert, W., & de Baar, H. J. W. (2008). A rapid transition from ice covered CO_2-rich waters to a biologically mediated CO_2 sink in the eastern Weddell Gyre. *Biogeosciences Discussions*, *5*, 1205–1235. http://dx.doi.org/10.5194/bgd-5-1205-2008.

Bakker, D. C. E., Pfeil, B., Smith, K., Hankin, S., Olsen, A., Alin, S. R., ... Watson, A. J. (2014). An update to the surface ocean CO_2 atlas (SOCAT version 2). *Earth System Science Data*, *6*(69–90), dli. http://dx.doi.org/10.5194/essd-6-69-2014.

Barbini, R., Fantoni, R., Palucci, A., Colao, F., Sandrini, S., Ceradini, S., & Tositti, L. (2003). Simultaneous measurements of remote lidar chlorophyll and surface CO_2 distributions in the Ross Sea. *International Journal of Remote Sensing*, *24*, 3807–3819.

Bates, N. R., Hansell, D. A., Carlson, C. A., & Gordon, L. I. (1998a). Distribution of CO_2 species, estimates of net community production, and air–sea CO_2 exchange in the Ross Sea polynya. *Journal of Geophysical Research*, *103*, 2883–2896.

Bates, N. R., Takahashi, T., Chipman, D. W., & Knap, A. H. (1998b). Variability of pCO_2 on diel to seasonal timescales in the Sargasso Sea near Bermuda. *Journal of Geophysical Research*, *103*, 15567–15585.

Bender, M. L., Ho, D. T., Hendricks, M. B., Mika, R., Battle, M. O., Tans, P. P., ... Cassar, N. (2005). Atmospheric O_2/N_2 changes, 1993–2002: implications for the partitioning of fossil fuel CO_2 sequestration. *Global Biogeochemical Cycles*, *19*, B4017.

Blain, S., Quéguiner, B., Armand, L., Belviso, S., Bombled, B., Bopp, L., ... Wagener, T. (2007). Effect of natural iron fertilization on carbon sequestration in the Southern Ocean. *Nature*, *446*(7139), 1070–1074.

Chen, L., Xu, S., Gao, Z., Chen, H., Zhang, Y., Zhan, J., & Li, W. (2011). Estimation of monthly air–sea CO_2 flux in the southern Atlantic and Indian Ocean using in-situ and remotely sensed data. *Remote Sensing of Environment*, *115*, 1935–1941.

Gruber, N., Gloor, M., Mikaloff Fletcher, S. E., Doney, S. C., Dutkiewicz, S., Follows, M. J., ... Takahashi, T. (2009). Oceanic sources, sinks, and transport of atmospheric CO_2. *Global Biogeochemical Cycles*, *23*, B1005.

H ales, B., & Takahashi, T. (2004). High-resolution biogeochemical investigation of the Ross Sea, Antarctica, during the AESOPS (U. S. JGOFS) Program. *Global Biogeochemical Cycles*, *18*, B3006.

Jiang, L., Cai, W., Wanninkhof, R., Wang, Y., & Lüger, H. (2008). Air–sea CO_2 fluxes on the U.S. South Atlantic Bight: Spatial and seasonal variability. *Journal of Geophysical Research*, *113*, C7019.

Jouandet, M. P., Blain, S., Metzl, N., Burnet, C., Trull, T. W., & Obernosterer, I. (2008). A seasonal carbon budget for a naturally iron-fertilized bloom over the Kerguelen Plateau in the Southern Ocean. *Deep-Sea Research Part II*, *55*, 856–867.

Le Quéré, C., Takahashi, T., Buitenhuis, E. T., Rödenbeck, C., & Sutherland, S. C. (2010). Impact of climate change and variability on the global oceanic sink of CO_2. *Global Biogeochemical Cycles*, *24*, B4007.

Lenton, A., Tilbrook, B., Law, R. M., Bakker, D., Doney, S. C., Gruber, N., ... Takahashi, T. (2013). Sea–air CO_2 fluxes in the Southern Ocean for the period 1990–2009. *Biogeosciences*, *10*, 4037–4054.

Louanchi, F., & Hoppema, M. (2000). Interannual variations of the Antarctic Ocean CO_2 uptake from 1986 to 1994. *Marine Chemistry*, *72*, 103–114.

Louanchi, F., Hoppema, M., Bakker, D. C. E., Poisson, A., Stoll, M. H. C., & De Baar, H. J. W. (1999). Modelled and observed sea surface fCO_2 in the Southern Ocean: a comparative study. *Tellus*, *B51*, 541–559.

McNeil, B. I., Metzl, N., Key, R. M., Matear, R. J., & Corbiere, A. (2007). An empirical estimate of the Southern Ocean air–sea CO_2 flux. *Global Biogeochemical Cycles*, *21*, B3011. http://dx.doi.org/10.1029/2007GB002991.

Metzl, N., Tilbrook, B., & Poisson, A. (1999). The annual fCO_2 cycle and the air–sea CO_2 flux in the sub-Antarctic Ocean. *Tellus*, *51B*, 849–861.

Orsi, A. H., Whitworth, T., III, & Nowlin, W. D., Jr. (1995). On the meridional extent and fronts of the Antarctic circumpolar current. *Deep-Sea Research Part I*, *42*, 641–673.

Pierrot, D., Neill, C., Sullivan, L., Castle, R., Wanninkhof, R., Lüger, H., ... Cosca, C. E. (2009). Recommendations for autonomous underway pCO_2 measuring systems and data-reduction routines. *Deep-Sea Research Part II*, *56*, 512–522.

Quay, P., Sonnerup, R., Stutsman, J., Maurer, J., Kortzinger, A., Padin, X. A., & Robinson, C. (2007). Anthropogenic CO_2 accumulation rates in the North Atlantic Ocean from changes in the $^{13}C/^{12}C$ of dissolved inorganic carbon. *Global Biogeochemical Cycles*, *21*, GB1009. http://dx.doi.org/10.1029/2006GB002761.

Rangama, Y., Boutin, J., Etcheto, J., Merlivat, L., Takahashi, T., Delille, B., ... Bakker, D. C. E. (2005). Variability of the net air–sea CO_2 flux inferred from shipboard and satellite measurements in the Southern Ocean south of Tasmania and New Zealand. *Journal of Geophysical Research*, *110*(C09005). http://dx.doi.org/10.1029/2004JC002619.

Sabine, C. L., Feely, R. A., Gruber, N., Key, R. M., Lee, K., Bullister, J. L., ... Rios, A. F. (2004). The oceanic sink for anthropogenic CO_2. *Science*, *305*, 367–371.

Sweeney, C. (2002). The annual cycle of surface water CO_2 and O_2 in the Ross Sea: a model for gas exchange on the continental shelves of Antarctic. *Biogeochemistry of the Ross Sea, Antarctic Research Series*, *78*, 295–312.

Takahashi, T., Feely, R. A., Weiss, R. F., Wanninkhof, R. H., Chipman, D. W., Sutherland, S. C., & Takahashi, T. T. (1997). Global air–sea fluxes of CO_2: an estimate based on measurements of sea–air pCO_2 difference. *Proceedings of the National Academy of Science. 94.* (pp. 8292–8299).

Takahashi, T., Sutherland, S. C., Sweeney, C., Poisson, A., Metzl, N., Tilbrook, B., ... Nojiri, Y. (2002). Global sea–air CO_2 flux based on climatological surface ocean pCO_2, and seasonal biological and temperature effects. *Deep-Sea Research Part II*, *49*, 1601–1622.

Takahashi, T., Sutherland, S. C., Wanninkhof, R., Sweeney, C., Feely, R. A., Chipman, D. W., ... de Baar, H. J. W. (2009). Climatological mean and decadal change in surface ocean pCO_2, and net sea–air CO_2 flux over the global oceans. *Deep-Sea Research Part II*, *56*, 554–577.

Takahashi, T., Sweeney, C., Hales, B., Chipman, D. W., Newberger, T., Goddard, J. G., ... Sutherland, S. C. (2012). The changing carbon cycle in the Southern Ocean. *Oceanography*, *25*, 26–37.

Tans, P. P., Fung, I. Y., & Takahashi, T. (1990). Observational constraints on the global atmospheric CO_2 budget. *Science*, *247*, 1434–1438.

Taylor, J. R. (1997). An introduction to error analysis: the study of uncertainties in physical measurements. (2nd ed.). *Univ. Sci. Books, Sausalito, Calif.* (327 pp).

Wanninkhof, R. (1992). Relationship between wind speed and gas exchange over the ocean. *Journal of Geophysical Research*, *97*, 7373–7382.

Wanninkhof, R. (2014). Relationship between wind speed and gas exchange over the ocean revisited. *Limnology and Oceanography: Methods*, *12*, 351–362.

Wanninkhof, R., Asher, W. E., Ho, D. T., Sweeney, C., & McGillis, W. R. (2009). Advances in quantifying air–sea gas exchange and environmental forcing. *Annual Review of Marine Science*, *1*, 213–244.

Weiss, R. F. (1974). Carbon dioxide in water and seawater: the solubility of a non-ideal gas. *Marine Chemistry*, *2*, 203–215.

Winguth, A. M. E., Heimann, M., Kurz, K. D., Marier-Reimer, E., Mikolajewicz, U., & Segschneider, J. (1994). El Nino Southern oscillation related fluctuations of marine carbon cycle. *Global Biogeochemical Cycles*, *8*, 39–63.

Worby, A. P., Geiger, C. A., Paget, M. J., Van Woert, M. L., Ackley, S. F., & Deliberty, T. L. (2008). Thickness distribution of Antarctic sea ice. *Journal of Geophysical Research*, *113*, C5S–C92S.

Xie, X., Wei, J., & Huang, L. (2014). Evaluation of ASCAT coastal wind product using nearshore buoy data. *Journal of Applied Meteorological Science*, *25*(4), 445–453.